Links between Tropical Convection and Variations of the Extratropical Circulation during TOGA COARE

GREG C. TYRRELL AND DAVID J. KAROLY

Cooperative Research Centre for Southern Hemisphere Meteorology, Monash University, Clayton, Victoria, Australia

JOHN L. MCBRIDE

Bureau of Meteorology Research Centre, Melbourne, Victoria, Australia

(Manuscript received 17 January 1996, in final form 23 April 1996)

ABSTRACT

Data from the Intensive Observation Period of the Tropical Ocean Global Atmosphere Coupled Ocean–Atmosphere Response Experiment (November 1992–February 1993) have been used to investigate the links between intraseasonal variations in tropical convection and those in forcing of upper-tropospheric Rossby waves in the extratropics. The primary databases are Geostationary Meteorological Satellite imagery and tropical wind analyses from the Bureau of Meteorology, Australia. A number of 5-day periods showing convection in different locations were chosen. For each period, mean fields of divergence, cloud-top temperature, and upper-tropospheric Rossby wave source are presented. Vorticity budgets are used to demonstrate the processes responsible for the Rossby wave source patterns. The approach follows earlier studies of links between interannual variations of tropical convection associated with the Southern Oscillation and variations of the extratropical circulation.

It is shown that the regions of tropical convection correspond to longitudinally localized Hadley cells. In the subtropics, at the higher-latitude end of each cell, there is a Rossby wave source dipole with anticyclonic and cyclonic forcing. The anticyclonic forcing of Rossby waves is associated with advection of vorticity by the divergent outflow, while the cyclonic forcing is due to the region of convergence immediately above the downward branch of the local Hadley cell. Hence, the authors provide a dynamical basis for tropical–midlatitude interactions associated with intraseasonal variations of tropical convection.

1. Introduction

The Tropical Ocean Global Atmosphere Coupled Ocean–Atmosphere Response Experiment (TOGA COARE) began in July 1992 with enhanced monitoring of the tropical western Pacific region and continued through June 1993 (Webster and Lukas 1992). We have used the comprehensive dataset provided by TOGA COARE to identify and investigate dynamical links between regions of enhanced tropical convection and anomalous extratropical circulation responses in the Southern Hemisphere on intraseasonal timescales. The period considered by this study is the four months of the COARE Intensive Observation Period (IOP), 1 November 1992–28 February 1993.

The large-scale atmospheric variability for this region during COARE has been documented by studies such as Gutzler et al. (1994) and McBride et al. (1995), who noted that there were two eastward progressions of enhanced convection across the region during the IOP, associated with the eastward propagating Madden–Julian oscillation (MJO). The MJO is the major influence on intraseasonal variations of convection in the western equatorial Pacific region and has been reviewed recently by Madden and Julian (1994).

It has become apparent that atmospheric circulation variability in both the Tropics and the extratropics is linked to large-scale changes in tropical heating over a broad frequency range. Kiladis and Weickmann (1992) examined atmospheric circulation anomalies associated with variations of tropical convection on three different intraseasonal timescales. They demonstrated that, during the northern winter, tropical convection in the 30–70, 14–30, and 6–14 day period bands was associated with statistically significant circulation anomalies in the Tropics and extratropics. Here, we investigate the dynamics of these linkages in a similar way to that used in studies of the Southern Oscillation (SO).

Many studies of the Southern Oscillation have demonstrated a linkage between tropical convection and the midlatitude circulation on interannual timescales. Horel and Wallace (1981) described observed correlations

Corresponding author address: Prof. David Karoly, CRC for Southern Hemisphere Meteorology, Monash University, Clayton, Victoria 3168, Australia.
E-mail: djk@vortex.shm.monash.edu.au

between various tropical time series and Northern Hemisphere geopotential height fields, while Hoskins and Karoly (1981) used a linearized baroclinic model to investigate the extratropical response to tropical heating. The proposal from such studies was that the extratropical response to tropical heating is due to Rossby wave propagation from a source located in the tropical upper troposphere.

In subsequent studies of the SO, Sardeshmukh and Hoskins (1988) and Rasmusson and Mo (1993) used the barotropic vorticity equation to diagnose Rossby wave sources at upper-tropospheric levels. Sardeshmukh and Hoskins (1988) demonstrated the importance of vorticity advection by the divergent flow in producing an effective Rossby wave source. Due to this mechanism, an equatorial region of tropical divergence situated in easterly winds could lead to a Rossby wave source in the subtropical westerlies where it could be extremely effective due to the presence there of large gradients in background absolute vorticity. Rasmusson and Mo (1993) showed that upper-level Rossby wave forcing could be remote from, but linked to, regions of tropical convection via localized Hadley circulations. Regions of extratropical convergence associated with the downward branch of local Hadley cells were found to be responsible for large Rossby wave forcing. Thus, regions of tropical convection and upper-level divergence, while not directly contributing to large Rossby wave sources in the Tropics, could indirectly lead to large regions of extratropical forcing via this mechanism.

Adopting methods from the above studies, this paper is aimed at investigating periods of varying tropical convection during the COARE IOP and establishing links to regions of enhanced extratropical Rossby wave forcing. Section 2 describes the data sources and analysis techniques used. Section 3 identifies and discusses the various 5-day periods considered, describing the tropical convection and features of the large-scale circulation during the IOP. The barotropic vorticity equation is used to diagnose extratropical Rossby wave forcing and its dynamical links with regions of tropical convection. Section 4 presents a budget analysis of the vorticity balance diagnostics, while section 5 summarizes the results.

2. Data sources and analysis procedures

a. Data sources

Gridpoint analysed data from two separate analysis schemes, the Bureau of Meteorology's Tropical Analysis Scheme (TAS) and the European Centre for Medium-Range Weather Forecasts (ECMWF) analyses, are used in conjunction with cloud property data from the Japanese Geostationary Meteorological Satellite (GMS).

TAS, described by Davidson and McAvaney (1981), is a three-dimensional univariate statistical interpolation scheme on a 2.5° latitude–longitude grid covering the domain from 45°N to 45°S, 80°E to 180°E. It has eight analysis levels up to 100 hPa with zonal and meridional winds, temperature, and moisture analyzed independently on sigma levels. Analyses are made twice daily at 1100 UTC and 2300 UTC using conventional surface and upper-air observations in addition to aircraft observations and satellite-derived cloud drift wind measurements. The scheme uses no model input and contains no dynamic constraints. The analysis technique involves correcting a first guess at any location using observations in the vicinity of the location and a history of temporal and spatial correlations between observations. For this scheme, the first guess is provided by 12-h persistence from the previous analysis. A large increase of meteorological observations due to COARE meant quality analyses could be made. Assessment of the scheme by Davidson et al. (1984) and Hendon (1988) has revealed that the analyzed fields, including divergence, are of high quality. Also, discussions by McBride et al. (1995) have demonstrated that time variations of the area-averaged divergence from TAS compare well with variations of tropospheric heating (calculated using networks of upper-air sounding data) and cloud-top temperatures (from the GMS) over various COARE regions.

Global analyses from ECMWF are also employed in this study to obtain comparisons with TAS. These data have also been obtained on a 2.5° latitude–longitude grid and have 14 levels up to 10 hPa, with zonal and meridional winds, temperature, and moisture analyzed on pressure levels. Described by Hollingsworth et al. (1985), the ECMWF analysis system uses a multivariate optimum interpolation scheme with a first guess from a 6-h forecast. The analysis is then used as the initial condition for the next 6-h forecast cycle.

Cloud Top Temperature (CTT) information obtained from the Japanese GMS is used in this study as an indicator of regions of deep tropical convection. The raw satellite data has been converted to blackbody temperatures according to Japanese Meteorological Agency lookup tables (Meteorological Satellite Center 1989). The cloud-based fields are obtained on a 2° latitude–longitude grid by averaging the blackbody temperature of individual pixels over a 50-km radius circle surrounding each grid point. The field employed in this study is CTT, defined as the average blackbody temperature value of all pixels in that grid circle.

b. Methodology

Diagnostics based on the analyzed wind fields from TAS were computed in order to identify various features of the large-scale circulation. Wind-based diagnostics including horizontal divergence (D), relative

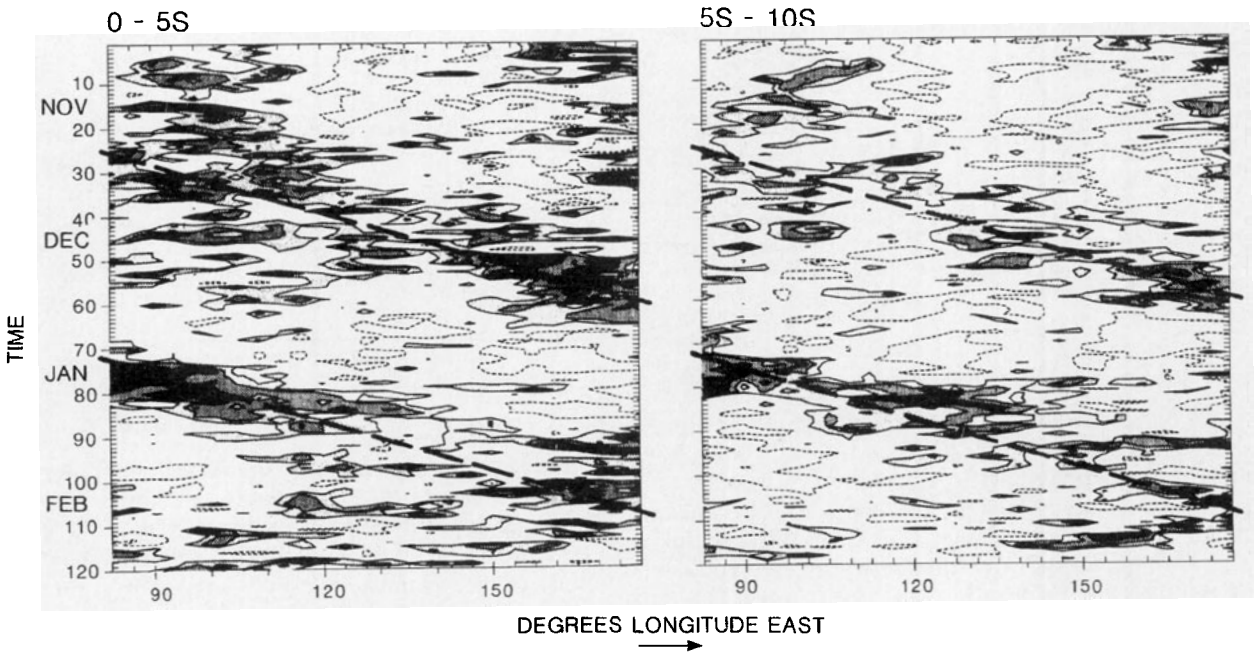

FIG. 1. Time–longitude strips of GMS cloud-top temperature. The domain is 80°E–180°, and strips are shown for two latitude bands. Cloud tops colder than −15°C are shaded. Phase lines for movement across the domain in 35 days (i.e., 3.7 m s^{-1}) are marked through the loci of the major regions of cloud. Reproduced from McBride et al. (1995).

vorticity (ζ), streamfunction (ψ), velocity potential (χ), and the divergent ($\mathbf{v}_\chi$) and rotational ($\mathbf{v}_\psi$) components of the wind have been calculated using finite difference methods on the TAS limited area grid.

Horizontal divergence and the vertical component of vorticity are solved first from the analyzed winds; ψ and χ are then calculated by solving the appropriate Helmholtz equations with the following boundary conditions: $\chi = 0$ and ψ, set by considering $\mathbf{v}_\psi$ equal to the analyzed wind component parallel to the boundary. These boundary conditions have been shown by Sangster (1960) to minimize the kinetic energy of the divergent wind over the domain. The technique, however, has been found to affect the solution close to the boundaries. Davidson et al. (1984) compared limited area domain analyses with global analyses and showed that, within 10° of the boundary, the solution is strongly affected by the imposed boundary conditions. However, they concluded that beyond 10° of the boundary of the analysis domain, solutions for $\mathbf{v}_\chi$ are sufficiently general to allow useful synoptic interpretation.

The basic parameters described here are calculated twice daily on the level $\sigma = 0.2$ and form the basis of many of the calculations presented in the following sections. Sigma levels are defined as atmospheric pressure/surface pressure, meaning that $\sigma = 0.2$ is very close to 200 hPa over the oceanic regions considered in this study. All terms have then been averaged into 5-day periods. Much of the intraseasonal signal is in the 30–60 day range and 5-day periods will capture nearly all of the intraseasonal time variations of the various diagnostics.

3. Tropical convection and vorticity forcing

According to McBride et al. (1995), variations in large-scale tropical convection on intraseasonal timescales during the IOP were governed by eastward progressions of two Madden–Julian events and by the development and subsequent movement of tropical cyclones in both (Northern and Southern) hemispheres. Figure 1, showing Hovmöller diagrams of CTT over 0°–5°S and over 5°–10°S for the COARE IOP, demonstrates this intraseasonal variability in tropical convection.

In this section, averaged fields are presented for seven 5-day periods with varying degrees of tropical convection. The degree and position of convection was inferred from 5-day fields of CTT with regions of CTT minima used to locate regions of deep convection in the analysis region (45°N–45°S, 80°E–180°). Table 1 provides a summary focussing on the dates, location, and strength of tropical convection for each of the seven periods. The cases have been ordered in time, with cases I–III and V–VII documenting the eastward passage of the two Madden–Julian events that occurred during the COARE IOP. Case IV occurred during the convectively inactive period separating the two events.

TABLE 1. Summary of 5-day averaged case periods, describing dates and location of tropical convection.

Case	Date	Description
I	1–5 Dec 1992	Strong equatorial convection to the west of the analysis region (~90°E)
II	11–15 Dec 1992	Two regions of strong equatorial convection located around longitudes 90°–115°E and 135°–165°E
III	21–25 Dec 1992	Convection located equatorially over much of the domain, but strongest activity in the eastern part (150°–170°E)
IV	10–14 Jan 1993	Very little tropical convection anywhere in the domain
V	15–19 Jan 1993	Strong tropical convection in the west of the domain near 90°E with some weaker convection to the east of the domain
VI	25–29 Jan 1993	Strong tropical convection in the center of the domain extending southward into the subtropics
VII	30 Jan–3 Feb 1993	Strong tropical convection covering the eastern half of the domain (130°–170°E) and extending southward into the subtropics over Australia

As discussed earlier, it is the aim of this study to investigate dynamic links between tropical convection and midlatitude vorticity forcing on intraseasonal timescales using the mathematical framework of Sardeshmukh and Hoskins (1988). Following Sardeshmukh and Hoskins (1988), the nonlinear vorticity equation at 200 hPa may be written

$$\left(\frac{\partial}{\partial t} + \mathbf{v}\cdot\nabla\right)(\zeta + f) = -(\zeta + f)D + \mathbf{k}\cdot\left(\frac{\partial \mathbf{v}}{\partial p} \times \nabla\omega\right) - \omega\frac{\partial \zeta}{\partial p} + F, \quad (1)$$

where ζ is the relative vorticity, f is the planetary vorticity, D is the horizontal divergence, $\mathbf{v}$ is the horizontal wind, ω is the vertical wind, and F is the frictional term. The strategy of Sardesmukh and Hoskins was to accumulate terms in this equation so that all terms necessary for the existence and propagation of Rossby waves are placed on the left-hand side. Then the remaining terms in the equation (now appearing on the right-hand side) can be referred to as Rossby wave sources (S) or as residual (i.e., not calculated) terms (R).

Decomposing the horizontal wind into rotational and divergent components, $\mathbf{v} = \mathbf{v}_\psi + \mathbf{v}_\chi$, the terms necessary for Rossby wave propagation involve local derivatives and advection of absolute vorticity by the rotational component of the flow. Thus, rewriting (1) gives

$$\left(\frac{\partial}{\partial t} + \mathbf{v}_\psi\cdot\nabla\right)(\zeta + f) = S + R. \quad (2)$$

Sardeshmukh and Hoskins (1988) found the twisting and vertical advection terms $\mathbf{k}\cdot(\partial\mathbf{v}/\partial p \times \nabla\omega)$ and $\omega(\partial\zeta/\partial p)$ of the full vorticity equation (1) to be negligible in comparison with the other terms. Thus, in this study these will not be calculated and, together with the frictional and subgrid-scale eddy term F, will make up the residual term R. This residual R also contains errors associated with the time-averaging and numerical procedures. Combining (1) and (2), this leaves the following form for the Rossby wave source:

$$S = -\mathbf{v}_\chi\cdot\nabla(\zeta + f) - (\zeta + f)\nabla\cdot\mathbf{v}_\chi. \quad (3)$$

This is the term used to investigate the effect of tropical convection on the midlatitude circulation via the forcing of upper-level Rossby waves diagnosed from observations. We wish to stress, however, that calculations of this quantity give only a diagnostic forcing for upper-tropospheric Rossby waves in the presence of divergence. Understanding how the atmosphere actually responds to these diagnosed forcings would require numerical experiments that are beyond the scope of the present study. Although we focus on divergence and convergence due to tropical convection, other processes such as baroclinic waves or radiative cooling could be responsible also for the divergence patterns, particularly in the subtropics and midlatitudes.

Below, maps are presented for various quantities including the two terms constituting S. To form the 5-day averages, each term is calculated at each grid point for each of the twice-daily individual maps and then averaged to represent the 5-day mean field. This was specifically to incorporate the effect of transient eddy terms in generation of upper-tropospheric Rossby waves.

In order to compress the discussion, one 5-day period will be discussed in detail to illustrate the main points. A short discussion will be given for the other six periods, basically to verify that the results are general. The 5-day period of 30 January–3 February 1993 has been chosen for detailed presentation. The discussion will also be limited to the Southern Hemisphere as there are some discrepancies between CTT and the analyzed divergence in the Northern Hemisphere, which might be expected as this is the winter hemisphere and upper-level divergence is not necessarily related to deep convection. Also, as will be seen, the regions in the Northern Hemisphere with large magnitude divergence generally lie close to the boundary of the analysis domain, where calculations of divergent component of flow are unreliable.

a. Case VII (30 January–3 February 1993)

Figure 2 shows (a) CTT, (b) D and $\mathbf{v}_\chi$, (c) $(\zeta + f)\nabla\cdot\mathbf{v}_\chi$, (d) $\mathbf{v}_\chi\cdot\nabla(\zeta + f)$, (e) S, and (f) ψ fields

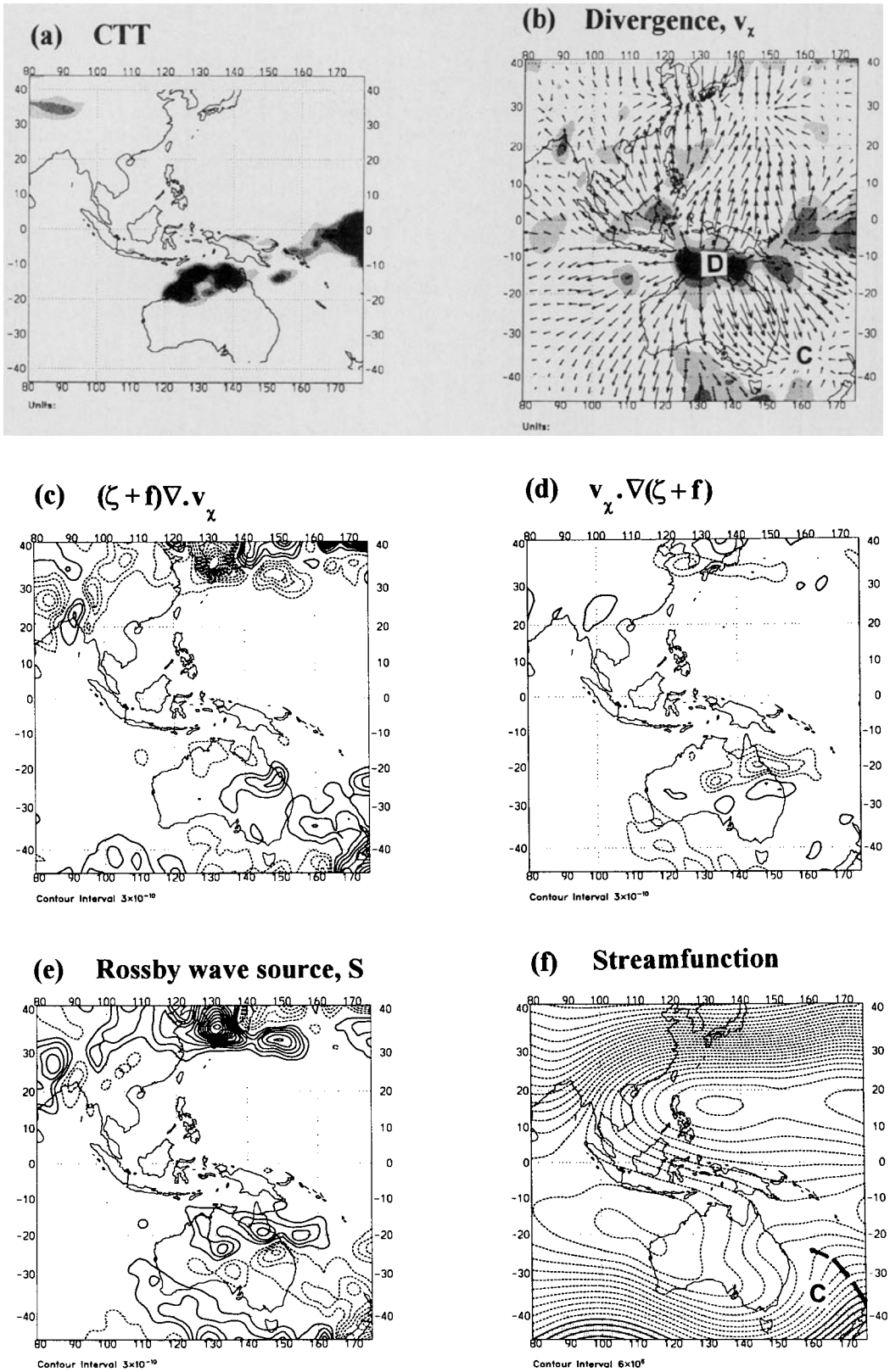

FIG. 2. Five-day average (a) CTT, (b) divergence D and $\mathbf{v}_\chi$, (c) $(\zeta + f)\nabla\cdot\mathbf{v}_\chi$, (d) $\mathbf{v}_\chi\cdot\nabla(\zeta + f)$, (e) Rossby wave source S, and (f) streamfunction ψ at $\sigma = 0.2$ for case VII, 30 Jan–3 Feb. Gray-scale shading indicates degree of CTT and divergence. Rossby wave source term contour plots have contour interval of 3×10^{-10} s^{-2}. Note that the zero contour line has been suppressed. The streamfunction contour plot has a contour interval of 6×10^{6} m^2 s^{-1}. Negative contours are dashed. The symbols C and D and the dashed lines are described in the text.

at $\sigma = 0.2$ for this 5-day period. The CTT map displays negative temperatures in terms of gray-scale shading, with darkest shading referring to regions of deepest convection. The divergence field is also displayed by gray-scale shading with regions of enhanced divergence identified by the darkest shading. The vector field overlayed on the divergence map is that of the divergent flow $\mathbf{v}_\chi$. The gray-scale shading of the CTT and divergence maps agree very closely in identifying regions of enhanced convection, particularly in the Tropics and the Southern Hemisphere.

This case was characterized by strong tropical convection covering the eastern part of the domain and captured a period during the passage of the second MJO. However, differing from the passage of the first MJO, this period demonstrated a more southern extension of convection into the subtropics over Australia associated with the Australian monsoon.

Upon inspection of the $\mathbf{v}_\chi$ field, the strongest vectors emanate from the regions of strongest convection and extend poleward to the north and south in regional Hadley cells. The magnitude of $\mathbf{v}_\chi$ is greater than 5 m s^{-1} in these strong outflow regions, which is comparable with or stronger than $\mathbf{v}_\psi$ in the same region. These localized Hadley circulations were first documented by Davidson et al. (1984). Later, Rasmusson and Mo (1993) described their importance in the generation of midlatitude Rossby waves associated with tropical convection. Following $\mathbf{v}_\chi$ from the convective centers, it can be seen that the Southern Hemisphere cells extend to regions of upper-level convergence around latitudes of 25°–35°S. Similar to these previous studies, these results demonstrate that upper-level convergence zones associated with the downward branches of Hadley cells tend to be localized rather than spread out uniformly over the globe. To make it easier to see the tie-in between the longitudinally localized Hadley cells and the Rossby wave source regions, the region of divergence delineating the source (or upward region) of the cell is marked with the letter *D*. Similarly, the convergent region at the poleward end is marked with the letter *C*.

The Rossby wave source term S and its two components, the vorticity-divergence stretching term $(\zeta + f)\nabla \cdot \mathbf{v}_\chi$ and the vorticity advection by the divergent wind term $\mathbf{v}_\chi \cdot \nabla(\zeta + f)$, have been directly computed from the TAS analyses, and the major features of these maps can be summarized as follows. To aid in interpretation, it is noted that cyclonic vorticity is negative in the Southern Hemisphere. Thus, a cyclonic source of Rossby waves appears as a negative (dashed contours) region on the map of total wave source (Fig. 2e). It is also noted that the source is equal to the negative of the two components in Figs. 2c and 2d.

Looking first at the total Rossby wave source (Fig. 2e), S is relatively small equatorward of about 20° and has larger values in the winter hemisphere. Thus, these 5-day patterns reveal a similar structure to the seasonal-mean patterns presented by Rasmussen and Mo (1993). Also, S has a dipole structure that ties in with the longitudinally localized Hadley cell in the Southern Hemisphere along the east coast of Australia (marked by the letters *D* and *C* in Fig. 2b). Specifically, in the convergent high-latitude end of the cell is a cyclonic Rossby wave source. Using Figs. 2c and 2d, it is seen that this is predominantly associated with the stretching term $(\zeta + f)\nabla \cdot \mathbf{v}_\chi$. It will be shown in the vorticity budgets in the following section that the main contribution to this is stretching of planetary vorticity, that is, $f\nabla \cdot \mathbf{v}_\chi$.

This result parallels the findings of Sardeshmukh and Hoskins (1988) and Rasmusson and Mo (1993) for longer timescales. Those authors demonstrated that regions of enhanced tropical convection and upper-level divergence do not directly contribute to large Rossby wave sources in the Tropics where the value of f approaches zero. However, links can be found between regions of tropical convection and extratropical areas of convergence via the regional Hadley cells. These regions of extratropical convergence appear to be very important in the generation of Rossby waves at upper levels.

Returning to the map of total S in Fig. 2e, the lower-latitude portion of the dipole is dominated by advection of absolute vorticity by the divergent flow, $\mathbf{v}_\chi \cdot \nabla(\zeta + f)$. This term was described by Sardeshmukh and Hoskins (1988) as being important in the correct specification of the Rossby wave source. Magnitudes of this term become comparable with the stretching term in the outflow region (10°–25°S, 145°–165°E) and depending on the sign of the vorticity gradient can cancel the effect of the stretching term. This is evident for this case where the stretching and advection terms are similar in magnitude but opposite in sense in the region of strong outflow from the convection. Similar to the stretching term, as the distribution of this term is largely dependent on the strength of the divergent wind, its location is highly sensitive to the location of tropical convection and of the subtropical convergence region.

Figure 2f shows the streamfunction field for this case. For ease in interpretation, the convergent region of the localized Hadley cell is also marked with a *C* on this figure. A wavelike response in the strong zonal flow is observed immediately downstream (east) of this region. This is marked on the figure by a dashed trough line and presumably is a response to the large cyclonic value of S that we have diagnosed in the convergence center.

It is apparent from the analyses that both the wave source and the observed generation of Rossby waves occur within 5 days of the associated period of maximum tropical convection. On the basis of these observations, it seems reasonable to suggest that for a local region, intraseasonal variations of tropical convection can directly lead to intraseasonal variations in the gen-

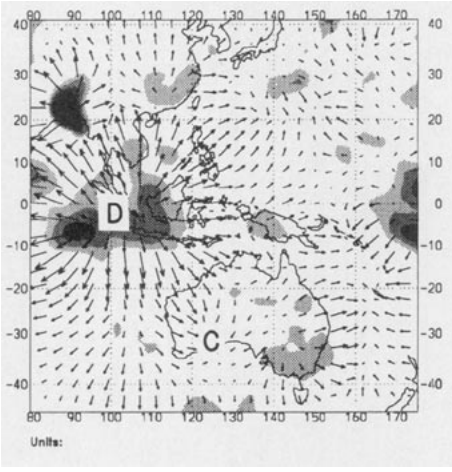

FIG. 3. Five-day average (a) divergence and v_χ, (b) S, and (c) ψ at $\sigma = 0.2$ for case I, 1–5 Dec. Gray-scale shading and contour intervals are identical to Fig. 2.

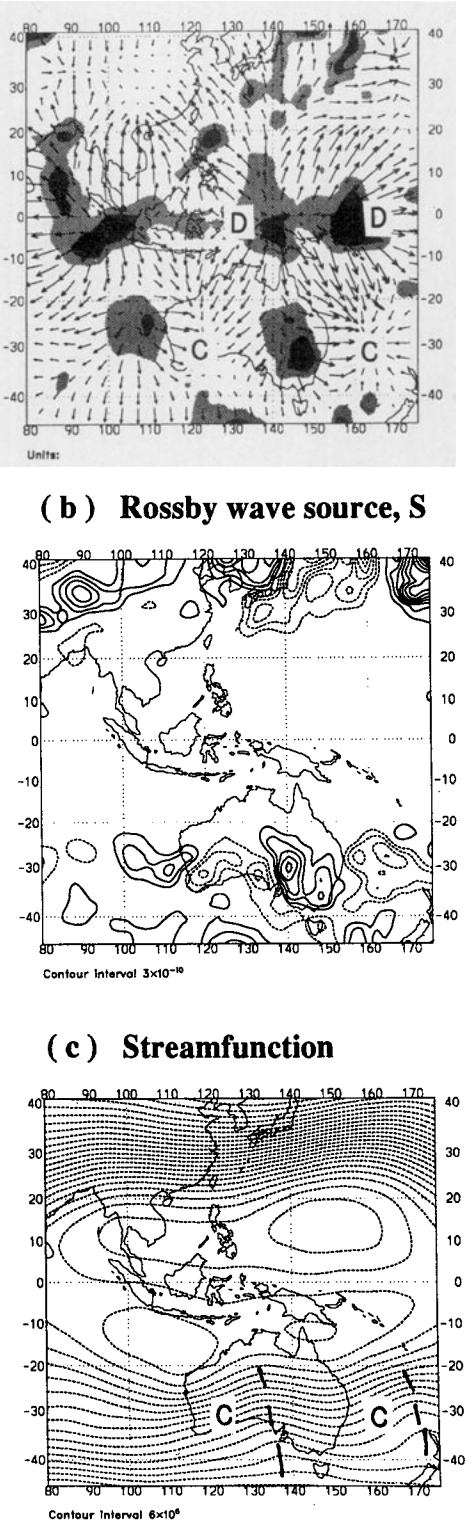

FIG. 4. As for Fig. 3 but for case II, 11–15 Dec.

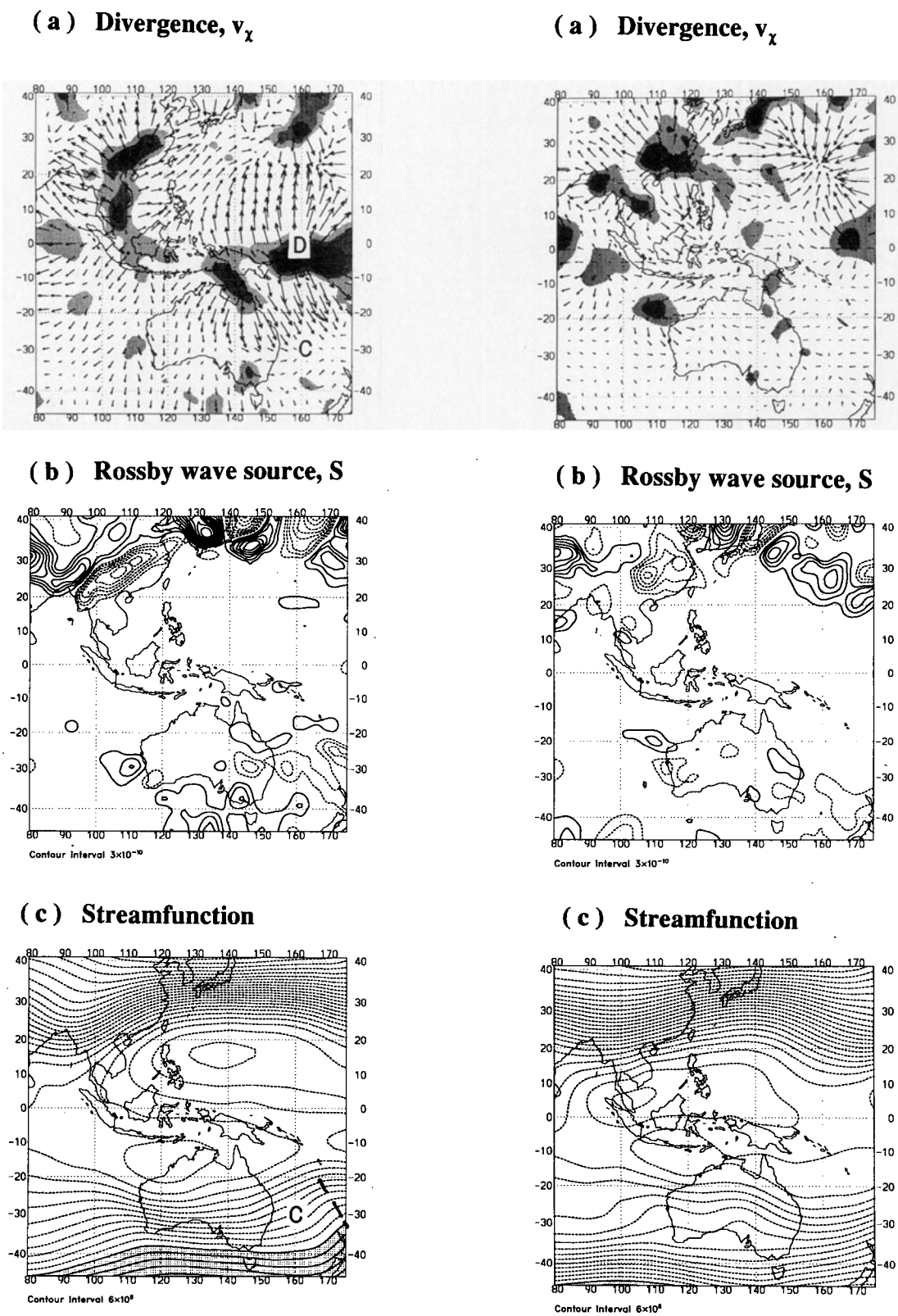

FIG. 5. As for Fig. 3 but for case III, 21–25 Dec.

FIG. 6. As for Fig. 3 but for case IV, 10–14 Jan.

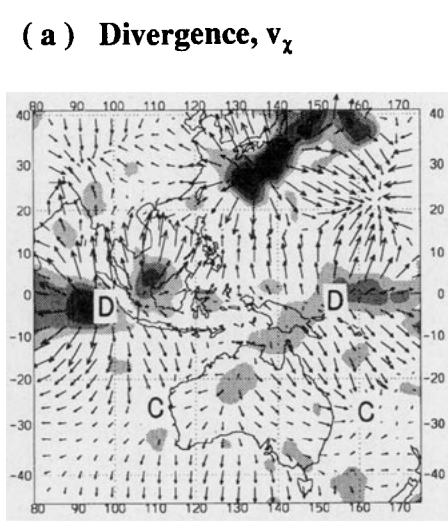

FIG. 7. As for Fig. 3 but for case V, 15–19 Jan.

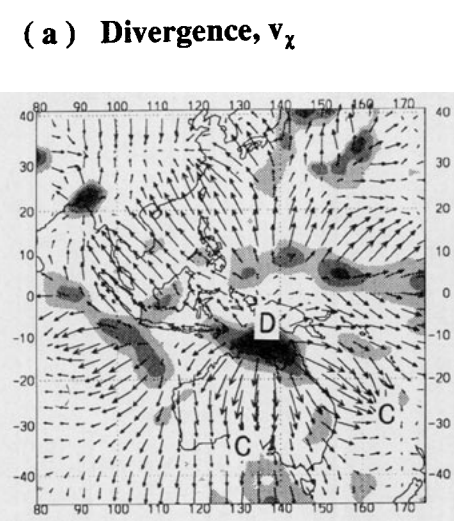

FIG. 8. As for Fig. 3 but for case VI, 30 Jan–3 Feb.

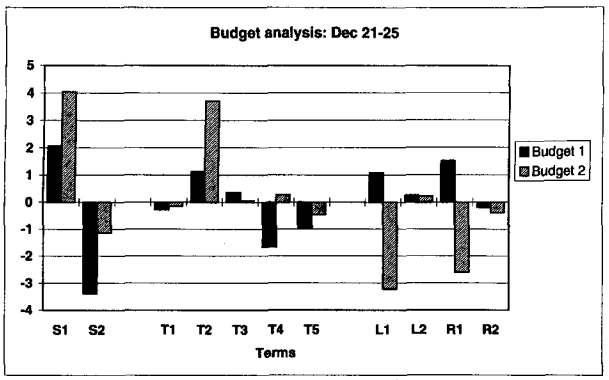

FIG. 9. Budget analysis of the barotropic vorticity equation using the TAS analyses for case III (21–25 Dec 1992). Terms are described in Table 2. Units are 10^{-10} s^{-2}. Budget 2 is for the higher latitude region of the Rossby wave source dipole (140°–170°E, 24.4°–29.6°S), while Budget 1 is for the region 140°–170°E, 19°–24.4°S.

eration of midlatitude vorticity sources and circulation in the local longitude belt. This hypothesis will be demonstrated further with a series of "snapshots" for each of the other six cases.

b. *Cases I–VI*

Figures 3–8 show (a) D and $\mathbf{v}_\chi$, (b) S, and (c) ψ at $\sigma = 0.2$ for cases I–VI, respectively. The position of tropical convection can be inferred from the divergence maps and localized Hadley circulations from the divergent flow. Similar to the above detailed case, regions of enhanced divergence and convergence have been labelled with "D" and "C" respectively for easier viewing.

The first of the intraseasonal oscillations in convection entered the western part of the domain in early December, and case I captures this period. As the oscillation propagates through the domain, cases II and III identify periods with convection based mainly around the center and later to the east of the domain. Consistent with the detailed case, case I shows a localized region of convergence (Fig. 3a) to the southeast of the enhanced tropical convection. Similarly located on the coast of Western Australia is a region of enhanced forcing (Fig. 3b) and a weak wavelike disturbance in the streamfunction (Fig. 3c). Case II actually displays two separate convectively active centers over Indonesia and Papua New Guinea, and these have been accurately depicted in the divergence field (Fig. 4a). As a result, two localized Hadley circulations and two regions of extratropical convergence off the east coast of Australia and central Western Australia can be identified for this period. Again, coinciding with these extratropical locations are two regions of large magnitude vorticity forcing (Fig. 4b). Also, the streamfunction field (Fig. 4c) suggests that an extratropical wavelike response to the tropical convection is present. Case III is similar to the detailed case in that it depicts a period when convection was located on the equator in the eastern part of the TAS domain. The enhanced tropical divergence (Fig. 5a) associated with convection did not extend as far south into the subtropics as the detailed case, and the region of subtropical convergence was located at slightly lower latitudes. Because of this, less Rossby wave forcing due to the $\mathbf{v}_\chi \cdot \nabla(\zeta + f)$ term was evident in the subtropics. However this period did display a strong local Hadley circulation and a large region of extratropical convergence associated with the convection. This region located around 30°S and 150°–170°E also demonstrates large-amplitude forcing (Fig. 5b) and a strong wavelike disturbance in the streamfunction (Fig. 5c).

Cases V and VI (Figs. 7 and 8) occur during the passage of the second MJO, when tropical convection was located to the west and center of the domain. Note that cases I and V (describing periods when convection was located to the west of the domain) do not exhibit the same strong response as the other cases in the extratropics. In fact, for both cases, the divergent flow from the convective regions does not demonstrate the same degree of localized convergence. It is not known if this is a characteristic for this region, if it is associated with midlatitude baroclinic wave activity, or whether it arises due to a lack of observational data in the area. Similar to the findings of the detailed case, however, the location and strength of extratropical vorticity forcing for most of these other cases is highly sensitive to variations in tropical convection.

Also, for most of the cyclonic (negative) vorticity sources seen in these cases, there is evidence of a dipole structure with a positive source immediately equatorward in the divergent flow. The interesting test case is IV (Fig. 6), which is for the convectively quiescent

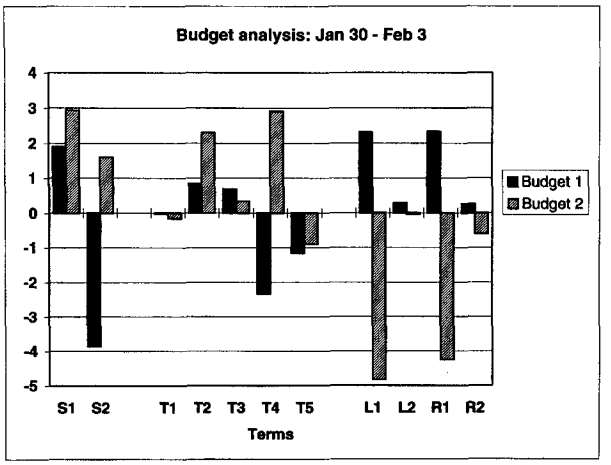

FIG. 10. As for Fig. 9 but for case VII, 30 Jan–3 Feb 1993.

TABLE 2. Description of terms constituting the vorticity budgets in Figs. 9–11.

S1 and S2 primary components of vorticity source

$S1 = \overline{(\zeta + f)\nabla\cdot\mathbf{v}}$

$S2 = \overline{\mathbf{v}_\chi\cdot\nabla(\zeta + f)}$

T1, T2, T3, T4, and T5 Subcomponents of vorticity source

T1 = transient term = $\nabla\cdot\overline{(\zeta'\mathbf{v}'_\chi)}$

T2 = stretching of planetary vorticity = $\overline{f\nabla\cdot\mathbf{v}}$

T3 = stretching of relative vorticity = $\overline{\nabla\cdot\mathbf{v}}$

T4 = divergent flow advection of relative vorticity = $\overline{\mathbf{v}_\chi}\cdot\nabla\overline{\zeta}$

T5 = divergent flow advection of planetary vorticity = $\overline{\mathbf{v}_\chi}\cdot\mathbf{v}f$

L1, L2, R1, and R2 complete budget

L1 = First term on the lhs of (2) = $\overline{\mathbf{v}_\chi\cdot\nabla(\zeta + f)}$

L2 = Second term on the lhs of (2) = $\partial\overline{\zeta}/\partial t$

R1 = First term on the rhs of (2) = Rossby wave source = $\overline{S}$

R2 = Second term on the lhs of (2) = budget residual = R

period. As would be expected, vorticity forcing is relatively small in comparison with the other cases. Despite this, one coherent vorticity source does appear off the Western Australian coast, which may be due to convergence in a baroclinic wave or to weak local convection. This vorticity source is also accompanied by weak downstream cyclonic waves, shown in the streamfunction in Fig. 6c.

4. Vorticity budget analysis

The individual terms of (2) have been calculated for two areas off the east coast of Australia for each of the seven cases. In addition, the Rossby wave source terms of the balance have been decomposed into transient and time-averaged terms as follows:

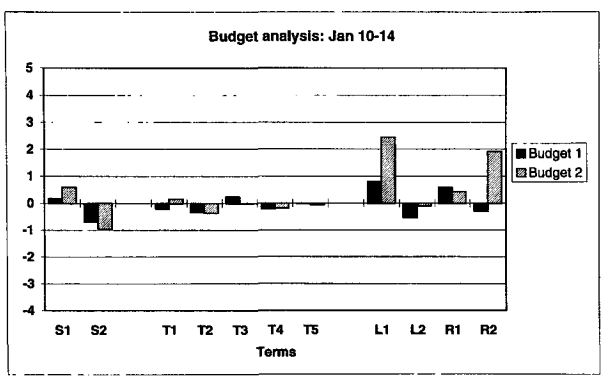

FIG. 11. As for Fig. 9 but for the nonconvective case IV, 10–14 Jan 1992.

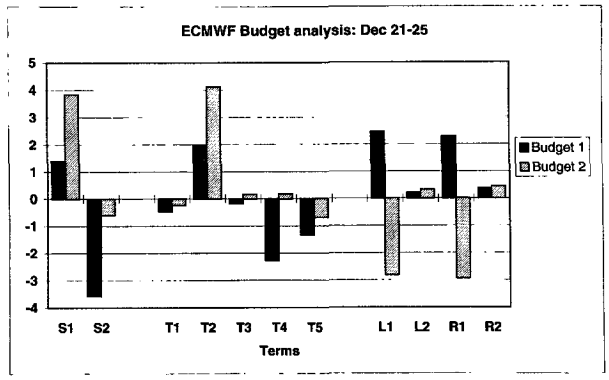

FIG. 12. As for Fig. 9 but with calculations derived from the ECMWF analyses for the same period (case III, 21–25 Dec 1992).

$$\overline{S} = \overline{(\zeta + f)D} + \overline{\mathbf{v}_\chi\cdot\nabla(\zeta + f)}$$
$$= f\overline{D} + \overline{\zeta}\overline{D} + \overline{\mathbf{v}_\chi}\cdot\nabla\overline{\zeta} + \beta\overline{\mathbf{v}_\chi} + \nabla\cdot\overline{(\zeta'\mathbf{v}'_\chi)}. \quad (4)$$

The purpose of this budget analysis is to assess the relative importance of each individual term. In addition, the magnitude of the residual between the left- and right-hand sides of the balance provides a sensitivity check on the consistency of the analyzed terms and, thus, on the interpretation of the results presented above.

Two budget areas were chosen to coincide with locations of significant Rossby wave forcing for the case presented in detail, case VII (30 January–3 February) and for case III (21–25 December). The budget boxes are located between longitudes 140°–170°E, and latitudes 19°–24.4°S (budget area 1) and 24.4°–29.6°S (budget area 2). From earlier discussions of these periods, it was anticipated that these two regions would provide budget analyses with different characteristics.

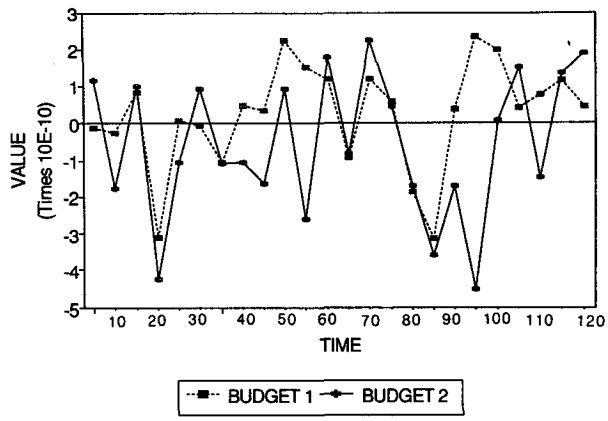

FIG. 13. Five-day-averaged Rossby wave source time series for budget 1 (dashed line) and budget 2 (solid line). Period of the time series covers the 120 days of the COARE IOP. Units are 10^{-10} s^{-2}.

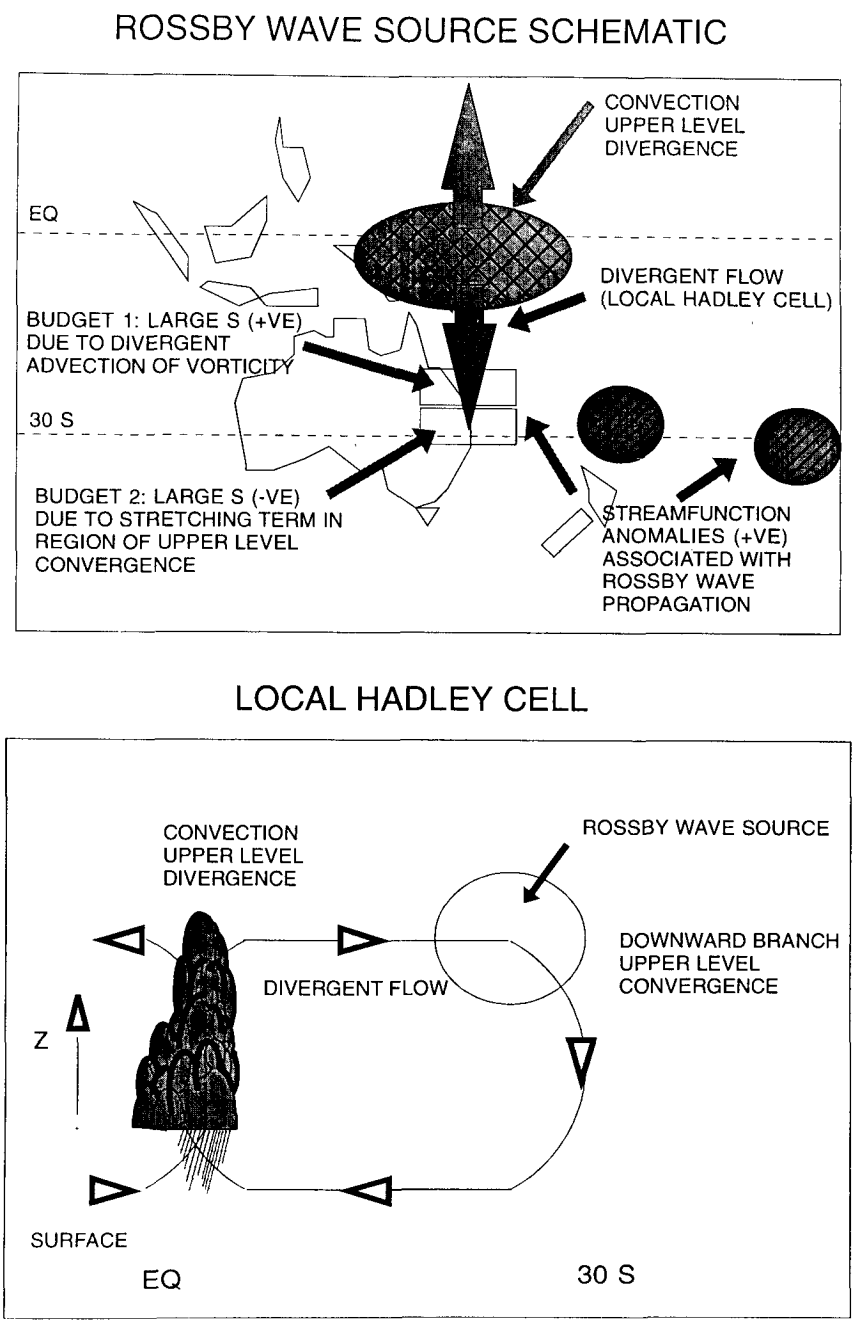

FIG. 14. (a) Schematic diagram demonstrating dynamical links between tropical convection and midlatitude Rossby wave sources in the Southern Hemisphere. (b) Schematic diagram of a local Hadley cell that links tropical convection to the midlatitudes.

Budget area 1 represents the positive (anticyclonic) part of the dipole and should be characterized by strong advection of vorticity by the divergent wind. Budget area 2 is chosen to represent the enhanced upper-level convergence and consequent compression of planetary vortex tubes, giving a negative vorticity source.

Figures 9 and 10 show the vorticity budgets for cases III and VII calculated from the TAS analyses. To aid in interpretation, the meaning of each term is outlined in Table 2. Both cases correspond to strong convective forcing situations, and the balance is primarily between the S and $\mathbf{v}_\psi \cdot \nabla(\zeta + f)$ terms (R1 and L2) as the $\partial\zeta/$

∂t and residual terms are relatively small. Hence, in extratropical regions of convergence associated with tropical convection, the divergent flow can be viewed as driving the upper-level rotational circulation via the generation and propagation of Rossby waves. It is noteworthy that this balance is maintained in both the anticyclonically forced (budget 1) and the cyclonically forced (budget 2) regions of the Rossby wave source dipole.

Figure 11 shows the budget for case IV, the nonconvective situation. Here, with no significant vorticity forcing anywhere, budget 2 displays a relatively large residual. As the individual terms in this case are relatively smaller than the other cases presented, it is likely that the contribution of the neglected terms could be important here. Hence, it would seem that the balance between the Rossby wave source and $\mathbf{v}_\psi \cdot \nabla(\zeta + f)$ is only valid in regions of enhanced forcing.

Referring back to the forced cases in Figs. 9 and 10, budgets 1 and 2 display different characteristics in terms of the relative importance of the two terms that contribute to the effective Rossby wave source. Closer to the equator (budget 1), the contribution from the $\mathbf{v}_\chi \cdot \nabla(\zeta + f)$ term (S2) is more important than the $(\zeta + f)\nabla \cdot \mathbf{v}_\chi$ term (S1) and opposite in sense. This term is negative in this region and as such generates a positive (anticyclonic) vorticity source. On the other hand, analysis of budget area 2, characterized by strong upper-level convergence, reveals that the $(\zeta + f)\nabla \cdot \mathbf{v}_\chi$ term (S1) is much more significant. Being positive in this region, the stretching term generates a negative (cyclonic) vorticity source. Due to the relatively large magnitude of this term and a lesser degree of cancellation with the advection term, the Rossby wave source has a maximum magnitude in this budget area.

Referring to the decomposition of the Rossby wave source terms, it is apparent that the $\overline{\mathbf{f}\nabla \cdot \mathbf{v}}$ and $\overline{\mathbf{v}_\chi} \cdot \overline{\nabla\zeta}$ terms (T2 and T4) are the most significant contributors to the stretching and advection terms, respectively. Further analysis of other terms reveals that the $\nabla \cdot \overline{(\zeta' \mathbf{v}'_\chi)}$, $\zeta \nabla \cdot \mathbf{v}$, and $\beta \mathbf{v}_\chi$ are relatively unimportant for most cases.

The accuracy of the vorticity balance diagnostics is confirmed by the relatively small residual between the left- and right-hand sides of the equation for cases III and VII. This would also indicate that the vertical advection, twisting, and frictional terms are relatively small in upper-level regions of Rossby wave forcing. To confirm the high quality of the TAS vorticity budgets, the vorticity budget for case III calculated from the ECMWF analyses is presented in Fig. 12. The ECMWF budget provides an independent estimate of the Rossby wave source and the residual and is very comparable with the TAS budget for this case. The differences between the Rossby wave sources and the residuals from the two budgets calculated from the different analyses provide an error estimate for the budget calculations. The relatively small residual term and the similarity between the TAS and ECMWF budgets indicate that the error estimates for the budgets are small. Thus, we can view the budget results with a fair degree of confidence.

As suggested earlier, observations have indicated that variations in tropical convection can directly lead to variations in the generation of midlatitude vorticity sources within a local longitude belt. With this in mind, a time series of the Rossby wave source S averaged over the two extratropical budget areas has been constructed to investigate how the source varies with time. The Rossby wave source time series for the two budget areas is displayed in Fig. 13 and consists of the 5-day-averaged source over the period of the COARE IOP. Remembering that for this longitudinal region, tropical convection peaked in late December (day 55) and again in early February (day 95), a similar MJO signal can be observed in the time series for budget 1. This is not surprising as this budget area is closer to the Tropics and S was primarily influenced by the $\mathbf{v}_\chi \cdot \nabla(\zeta + f)$ term directly associated with tropical convection and upper-level divergence. The same signal also exists in the source time series for budget area 2 to the extent that S has large negative magnitudes during periods of enhanced convection (days 55 and 95). This feature of positive $\mathbf{v}_\chi \cdot \nabla(\zeta + f)$ and negative $(\zeta + f)D$ during periods of enhanced local convection was shown by the dipole patterns in the Rossby wave source maps. Apart from a couple of exceptions, maximum positive values in the budget 1 time series and largest negative values in the budget 2 time series occur in the same periods associated with maximum tropical convection. However, there are some 5-day periods for both time series that are exceptions to the observations above. Large negative values for S in both time series occur on days 20 and 85 and may have been generated by midlatitude systems.

5. Discussion

Adopting methods from Sardeshmukh and Hoskins (1988) and Rasmusson and Mo (1993), this study has considered Rossby wave sources and midlatitude circulation responses at upper levels associated with various 5-day periods of tropical convection during the COARE IOP. Concentrating on the Southern Hemisphere, this study has been able to identify localized Hadley cells emanating from regions of tropical convection and extending into the extratropics. These local Hadley cells form direct links between regions of tropical convection and regions of enhanced Rossby wave forcing in the extratropics. The main findings are synthesized into the two schematic diagrams in Fig. 14.

The top diagram shows that major outbreaks of tropical convection are associated with longitudinally localized Hadley cells extending into the subtropics in

both (Northern and Southern) hemispheres. Near the low-latitude source of the cell, upper-tropospheric Rossby wave forcing is weak as both absolute vorticity and its gradient are small in magnitude. Toward the high latitude end of the cell is a region of large Rossby wave forcing in an anticyclonic sense. This is associated mainly with advection of relative vorticity by the divergent flow, that is, $\mathbf{v}_\chi \cdot \nabla\zeta$. At the high latitude end of the cell is an upper-level region of convergence. This corresponds to an area of large magnitude Rossby wave source S at upper levels, brought about by stretching of planetary vorticity $f\nabla \cdot \mathbf{v}$. Immediately downstream of this source, wavelike perturbations are observed in the streamfunction field, presumably in response to this Rossby wave source. As depicted in the diagram, the structure of these waves is such that they would correspond to a series of positive anomaly centers in the streamfunction field.

The lower schematic shows a cross-sectional view of the localized Hadley cell and serves to illustrate the point that the significant Rossby wave forcing is well removed from the upper-level divergence source. It also illustrates that the location of the Rossby wave forcing is immediately over the high-latitude downward branch of the cell.

These results extend those of earlier authors. In particular, they offer a dynamical explanation of linkages between intraseasonal variations of tropical convection and associated midlatitude circulation anomalies described by Kiladis and Weickmann (1992). The longitudinally localized Hadley cells were first noted in the Australian–western Pacific region by Davidson et al. (1984). Those authors described them in the context of the lower-level branch of the cell causing a forcing of tropical convective variations in response to midlatitude synoptic events. In the current study, we have demonstrated that the upper-level branch of the cell is associated with a forcing in the opposite direction, that is, midlatitude Rossby waves in response to tropical convection.

Acknowledgments. This study makes use of data collected during the TOGA COARE program, and we are grateful for the efforts of the large number of scientists from many countries that made this program so successful. Funding for the participation by Monash University in COARE was provided by an ARC Collaborative Research Grant, which also supported graduate study by GCT. DJK was supported by a grant from the Australian Cooperative Research Centres Program.

We are honored that this study was selected for inclusion in this special issue. Tsvi Gal-Chen spent several weeks visiting Monash University about ten years ago, and it was good to renew his acquaintance at the COARE Data Workshop in Toulouse in August 1994. This research was discussed with Tsvi there, and he was keenly interested, as always, in any aspect of atmospheric dynamics.

REFERENCES

Davidson, N. E., and B. J. McAvaney, 1981: The ANMRC tropical analysis scheme. *Aust. Meteor. Mag.*, **29,** 155–168.

——, J. L. McBride, and B. J. McAvaney, 1984: Divergent circulations during the onset of the 1978–79 Australian monsoon. *Mon. Wea. Rev.*, **112,** 1684–1696.

Gutzler, D. S., G. N. Kiladis, G. A. Meehl, K. M. Weickmann, and M. Wheeler, 1994: Seasonal climate summary: The global climate of December 1992–February 1993. Part II: Large-scale variability across the tropical western Pacific during TOGA COARE. *J. Climate,* **7,** 1606–1622.

Hendon, H. H., 1988: A qualitative assessment of the Australian tropical region analyses. *Mon. Wea. Rev.*, **116,** 5–17.

Hollingsworth, A., A. C. Lorenc, M. S. Tracton, K. Arpe, G. Cats, S. Uppala, and P. Kallberg, 1985: The response of numerical weather prediction systems to FGGE level IIb data. Part I: Analyses. *Quart. J. Roy. Meteor. Soc.*, **111,** 1–66.

Horel, J. D., and J. M. Wallace, 1981: Planetary-scale atmospheric phenomena associated with the Southern Oscillation. *Mon. Wea. Rev.*, **109,** 813–829.

Hoskins, B. J., and D. J. Karoly, 1981: The steady linear response of a spherical atmosphere in thermal and orographic forcing. *J. Atmos. Sci.*, **38,** 1179–1196.

Kiladis, G. N., and K. M. Weickmann, 1992: Circulation anomalies associated with tropical convection during northern winter. *Mon. Wea. Rev.*, **120,** 1900–1923.

Madden, R., and P. Julian, 1994: Observations of the 40–50-day tropical oscillation—A review. *Mon. Wea. Rev.*, **122,** 814–837.

McBride, J. L., N. E. Davidson, K. Puri, and G. C. Tyrrell, 1995: The flow during TOGA COARE as diagnosed by the BMRC tropical analysis and prognosis system. *Mon. Wea. Rev.*, **123,** 717–736.

Meteorological Satellite Center, 1989: *The GMS User's Guide.* 2d ed. Meteorological Satellite Center, 222 pp.

Rasmusson, E. M., and K. Mo, 1993: Linkages between 200-mb tropical and extratropical circulation anomalies during the 1986–1989 ENSO cycle. *J. Climate,* **6,** 595–616.

Sangster, W. E., 1960: A method of representing the horizontal pressure force without reduction of pressures to sea level. *J. Meteor.*, **17,** 166–176.

Sardeshmukh, P. D., and B. J. Hoskins, 1988: The generation of global rotational flow by steady idealized tropical divergence. *J. Atmos. Sci.*, **45,** 1228–1251.

Webster, P. J., and R. Lukas, 1992: TOGA COARE: The Coupled Ocean–Atmosphere Response Experiment. *Bull. Amer. Meteor. Soc.*, **73,** 1377–1417.